Journal of Nonlinear Waves (2026), **2**, e12, 1–18
doi:10.1017/jnw.2026.10038

CAMBRIDGE UNIVERSITY PRESS

RESEARCH ARTICLE

Localized pattern formation for mussel–algae model and other reaction-diffusion systems with saturation

Theodore Kolokolnikov[1], Shuanquan Xie[2] and Juncheng Wei[3]

[1]Department of Mathematics and Statistics, Dalhousie University, Halifax, NS, Canada
[2]Department of Mathematics, Hunan University, Changsha, China
[3]Department of Mathematics, Chinese University of Hong Kong, Hong Kong
Corresponding author: Theodore Kolokolnikov; Email: tkolokol@gmail.com

Keywords: asymptotic methods; pattern formation; reaction-diffusion systems

(Received 10 December 2025; revised 3 April 2026; accepted 21 April 2026)

Abstract
We examine a class of reaction-diffusion systems where saturation drives pattern formation. A prime example is the classical model of mussel–algae interactions. We asymptotically construct a pattern consisting of N spikes. Unlike many other models where the inner spike profile is described by a *nonlinear* ODE $w'' - w + w^p = 0$, here it is described by a *linear* ODE $w'' + w - 1 = 0$. We then study the stability of the resulting patterns. A new non-local eigenvalue problem is derived which controls the structural stability of N such spikes. We rigorously prove its stability in the relevant regime, taking advantage of the explicit formula for the shape of the spike. Self-replication is also observed, and we derive a new 'core problem' which captures this phenomenon. Finally, the asymptotic stability band for the existence of N spikes is given. Our methods are applicable to a wide range of systems that exhibit saturation; we provide a variant of the Schnakenberg model as another example. Numerical simulations confirm our asymptotic predictions.

1. Introduction

In this paper, we examine localized patterns for some reaction-diffusion systems driven by saturation or Allee effects. These are often included in population models in order to account for the effect of population size on predation or nutrient consumption. Consider the following variant of the well-known model of mussel–algae interactions [4, 27, 25, 42]:

$$M_t = d_1 M_{xx} - \frac{k_1}{k_2 + M} M + k_3 AM, \quad A_t = d_2 A_{xx} - VA_x + k_4 - k_5 A - k_6 AM. \tag{1.1}$$

The same model but with $k_5 = 0, V = 0$, was also studied in, e.g. [14, 35], from the point of view of chemical reactions with saturation. The mussel death rate $\frac{k_1}{k_2+M}$ decreases with higher density, reflecting a 'strength in numbers' protection mechanism. All parameters are assumed to be positive; see papers [25, 42] for a detailed explanation of the model and parameters. The path to pattern formation through Turing bifurcation is well understood for this and related models. In particular, the saturation is essential for the formation of spatial patterns in (1.1) (no spatial patterns are possible when saturation $\frac{k_1}{k_2+M}$ is replaced by k_1). Our goal here is to study localized patterns that arise far from the Turing bifurcation threshold. This is in contrast to numerous existing studies of this model, where the patterns are typically studied close to the Turing bifurcation threshold.

© The Author(s), 2026. Published by Cambridge University Press. This is an Open Access article, distributed under the terms of the Creative Commons Attribution licence (http://creativecommons.org/licenses/by/4.0), which permits unrestricted re-use, distribution and reproduction, provided the original article is properly cited.

https://doi.org/10.1017/jnw.2026.10038 Published online by Cambridge University Press

Many models of vegetation patterns incorporate saturation for both nutrients and plant biomass [11, 13, 37]. Among the simplest examples, consider the following variant of the classical Klausmeier model:

$$v_t = d_2 v_{xx} - k_4 v + \frac{k_5 v}{k_6 v + k_7} vu, \quad u_t = d_1 u_{xx} + k_1 - k_2 u - k_3 uv. \tag{1.2}$$

Here, v represents the biomass density and u the density of water. The water absorption rate by the plants $\frac{k_5 v}{k_6 v + k_7}$ is assumed to saturate with increased biomass density.

Both of these models have complex spatial patterns made up of spikes, as illustrated in Figures 1 and 5. We are interested in certain limits of the models (1.2) and (1.1) where the saturation plays a key role. As with most other studies of spike patterns, the basic building block is the asymptotic profile of the spike. In almost all other studies, this profile satisfies a *nonlinear* ODE of the form $w'' - w + w^p = 0$. By contrast, when saturation dominates, we find a new *linear* ODE for the ground state in the inner region, of the form $w'' + w - 1 = 0$. This is then matched to the outer region to construct the full spike profile.

As we will see later, saturation can have a profound effect on the resulting spatial patterns. The original paper of Klausmeier [17] assumed no saturation ($k_6 = 0$ in (1.2); though the Klausmeier model also included drift terms such as u_x in the equation for u to account for the flow of water downhill, which we are not considering here). In this case, the model (1.2) is equivalent to the Gray–Scott model or the Schnakenberg model (when $k_2 = 0$) which has been intensively studied from the point of view of localized patterns. There is a large literature on the subject; we refer to the book [45] and references therein for review.

Similar localized patterns have been studied in many other reaction-diffusion models. Some prominent examples include the Gray–Scott model [9, 20, 29, 32, 34, 36], the Schnakenberg model [3, 16, 23], vegetation patches in arid environments [7, 10, 17, 38–40], crime hot-spots in a model of residential burglaries [5, 22, 41, 46] and animal skin patterns [2, 12, 24, 26, 28, 33]. We single out the paper [15], which is the first to give the full description of stability of N spikes for the related Gierer–Meinhardt model. The framework developed in that paper forms the basis for stability analysis in this work.

The summary of the paper is as follows. Section 2 is dedicated to the analysis of the model (1.1). We construct the equilibrium spike profile in Section 2.1. We then study the stability of a pattern consisting of N identical copies of a spike in Section 2.2. As in the classical analysis [15], there are two types of eigenvalues to consider: large eigenvalues which correspond to structural stability of the pattern, and small eigenvalues that arise due to translation invariance of the inner region and are related to slow spike dynamics. We find a novel non-local eigenvalue problem (NLEP) (3.1) which describes the stability of spikes with respect to large eigenvalues, and proves their (in)stability depending on problem parameters. We then derive small-eigenvalue instability thresholds directly, by constructing asymmetric spike patterns. As with other models, we find that the competition instability – responsible for spike disintegration – is triggered due to small eigenvalue instabilities. In Section 2.3, we derive the so-called core problem, which captures the spike self-replication observed in (1.1). The stability of NLEP problem is analysed rigorously in Section 3. Section 4 is devoted to a similar analysis for the model (1.2). We conclude with a discussion and open problems in Section 5.

2. Mussel–algae model

We illustrate our technique on the mussel–algae model (1.1). Simulations of the steady state (see Figure 1) show the existence of spike patterns, corresponding to localized concentrations of the mussel population. We will first non-dimensionalize equations (1.1) as follows. Let $M = k_2 v$; $A = \frac{k_1}{k_2 k_3} u$; $t = \frac{k_2}{k_1} \tilde{t}$. After dropping the tilde we obtain

$$v_t = \varepsilon^2 v_{xx} + uv - \frac{v}{1+v}; \quad \tau u_t = D u_{xx} - D_2 u_x + a - bu - uv \tag{2.1}$$

https://doi.org/10.1017/jnw.2026.10038 Published online by Cambridge University Press

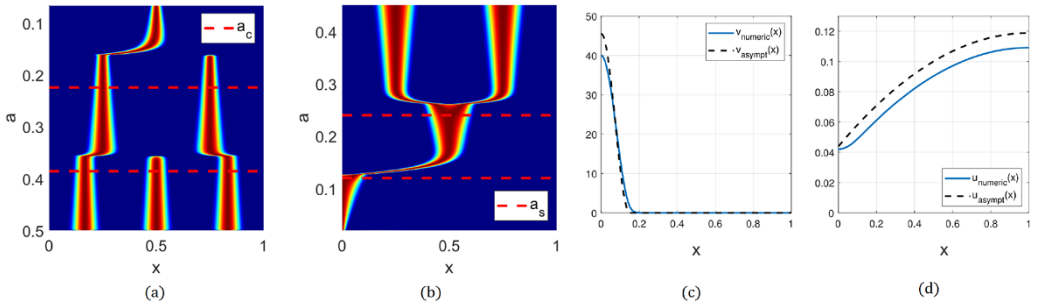


Figure 1. *(a) Spike competition instability for the model (2.3). Here, $D = 1$, $\varepsilon = 0.0015$, and a is gradually decreased according to $a = 0.5 - 10^{-5}t$. The number of spikes decreases as a decreases. Dashed line a_c shows the asymptotic threshold given by (2.5). Colouration is normalized at each time slice, with deep red corresponding to a maximum and deep blue corresponding to zero. (b) Self-replication. Parameters are the same as in (a) except a is gradually increased according to $a = 0.02 + 10^{-5}t$. The number of spikes increases as a increases. Asymptotic value for a_s given by (2.4) is also shown. (c) and (d) Half-spike steady state of (2.4), which is a basic building block of patterns. Here, $a = 0.15$, $\varepsilon = 0.01$, $l = 1, D = 1$. Panel (c) shows $v(x)$ and panel (d) shows $u(x)$. Dashed lines indicate asymptotics (2.15).*

where

$$a = \frac{k_4 k_3}{k_1 k_6}, \quad b = \frac{k_5}{k_6 k_2}, \quad \tau = \frac{k_1}{k_2 k_6 k_2}, \quad D = \frac{d_2}{k_6 k_2}, \quad V_u = \frac{V}{k_6 k_2}, \quad \varepsilon = \sqrt{\frac{d_1 k_2}{k_1}}. \tag{2.2}$$

In particular, the parameters used in [25, 42] yield the values $\varepsilon = 0.158$, $D_2 = 360$, $D = 0$, $\tau = 0.000131$, $a = 0.7$, $b = 0.6666$.

To simplify the calculation and illustrate key points, we will only look at the regime where the natural death rate of algae is negligible compared to death due to mussel consumption, and take $b = 0$. In addition, we will assume no drift: $D_2 = 0$. Note, however, our analysis can be extended to remove these assumptions. Moreover, we assume that the algae population changes on a faster timescale than the mussel population: $\tau \ll 1$, consistent with parameters in [25, 42] (which give $\tau = 0.000131$). With these assumptions, we write the simplified model in the form

$$v_t = \varepsilon^2 v_{xx} + uv - \frac{v}{1+v}; \quad 0 = Du_{xx} + a - uv. \tag{2.3}$$

We will also assume that the ratio of diffusion coefficients ε^2/D is small; in other words, the mussels move much slower than the algae. This is biologically reasonable, consistent with parameters as given, for example, in [25, 42] (there, drift u_x was used instead of the diffusion u_{xx} here; but very similar analysis is possible in that case), and allows for the decoupling of the spatial scales for v and u.

2.1. Steady state

Let us first construct a steady state for the model (2.3) asymptotically. It satisfies

$$0 = \varepsilon^2 v_{xx} + uv - \frac{v}{1+v}; \quad 0 = Du_{xx} + a - uv. \tag{2.4}$$

We remark that the equations for the steady state are the same even when τ is not assumed to be zero in (2.3); however non-zero τ complicates the analysis of stability and is a subject of future work. A typical steady state is shown in Figure 1 (c and d). We start by constructing a steady state consisting

https://doi.org/10.1017/jnw.2026.10038 Published online by Cambridge University Press

of a half-spike on the domain $[0, l]$. By even reflections, this can be extended to N symmetric interior spikes on the domain $(-l, (2N-1)l)$ of size $L = 2Nl$.

The steady state is divided into two regions: the *inner* region inside the spike and the *outer* region (refer to Figure 1 (c and d)). The analysis is done separately in both regions, along with asymptotic matching to resolve for unsolved constants.

In the inner region, we look for a solution of the form

$$y = \frac{\sqrt{u_0}}{\varepsilon}x, \; v = \frac{1}{u_0}V(y), \quad u(x) = U(y) \tag{2.5}$$

where $u_0 = U(0)$ is the value of $u(x)$ at the centre of the spike to be determined. Equation for $U(y)$, at leading order, becomes $U_{yy} \sim 0$. It follows that $U(y) \sim u_0 + By$. Standard asymptotic matching requires that $U(y)$ remains bounded as $y \to \infty$, so that $B = 0$. It follows that $U(y) \sim u_0$ is constant (with u_0 to be determined) in the inner region to leading order (note that $u(x)$ itself is non-constant, it is only constant to leading order inside the inner region).

Equation for $V(y)$ then becomes

$$V_{yy} + V - \frac{V}{u_0 + V} = 0. \tag{2.6}$$

Multiplying by V_y and integrating we obtain

$$\frac{V_y^2}{2} + \frac{V^2}{2} - V + u_0 \log(V + u_0) = C. \tag{2.7}$$

Assuming that $V(y) \to 0$ as $y \to \pm\infty$, we obtain $C = u_0 \log(u_0)$ so that (2.7) becomes

$$\frac{V_y^2}{2} + \frac{V^2}{2} - V + u_0 \log(V/u_0 + 1) = 0. \tag{2.8}$$

By assumption, $v(x)$ is symmetric with respect to $x = 0$, so that $V(y)$ has a maximum $V_{\max}$ at $y = 0$, $V_{\max} = V(0)$. Then $V_{\max}$ satisfies

$$\frac{V_{\max}^2}{2} - V_{\max} + u_0 \log(V_{\max}/u_0 + 1) = 0. \tag{2.9}$$

We are interested in the limit $u_0 \to 0$, which we assume to be true throughout this construction. This will impose certain self-consistency conditions on other parameters that will become clear below when u_0 is solved for below through matching (see (2.13) and (2.16)). Then (2.9) simplifies to

$$\frac{V_{\max}^2}{2} - V_{\max} \sim 0, \tag{2.10}$$

so that $V_{\max} \sim 2$ as $u_0 \to 0$. Furthermore, in the limit $u_0 \to 0$, the original equation (2.6) becomes

$$V_{yy} + V - 1 \sim 0 \tag{2.11}$$

Consequently, we obtain $V \sim 1 + A\cos(y)$. Moreover, $V(0) = V_{\max} = 2 = 1 + A$; this yields $V \sim 1 + \cos(y)$. The approximation (2.11) breaks down when $V = O(u_0)$, in other words, when $y \sim \pi$; an additional boundary layer near $y = \pi$ exists to resolve the transition from (2.11) to (2.6).[1]

[1]This additional layer can be analysed via a change of variables $V(y) = u_0\hat{V}(\hat{y})$, $\hat{y} = u_0(y - \pi)$; upon substituting into (2.4) we obtain, to leading order, $\hat{V}_{\hat{y}\hat{y}} - \frac{\hat{V}}{1+\hat{V}} = 0$. Expanding $V(y) \sim 1 + \cos(y) = 1 + \cos(\pi + u_0^{1/2}\hat{y}) \sim u_0\hat{y}^2/2$ gives the matching condition $\hat{V}(\hat{y}) \sim \hat{y}^2/2$

https://doi.org/10.1017/jnw.2026.10038 Published online by Cambridge University Press

Finally, in the outer, we assume that u and v are both small (which imposes a further constraint on parameter a to be determined, see below); the leading order for (2.4) then reads $\varepsilon^2 v_{xx} - v \sim 0$ so that v exhibits a fast exponential decay. Subsequently, to leading order, we obtain the spike profile of the form

$$v(x) \sim \frac{1}{u_0} \begin{cases} 1 + \cos\left(\frac{\sqrt{u_0}}{\varepsilon} x\right), & 0 \le x < \pi \frac{\varepsilon}{\sqrt{u_0}} \\ 0, & \text{otherwise} \end{cases}. \tag{2.12}$$

Finally, to obtain u_0, we integrate equation for u in (2.3) to obtain $al \sim u_0 \int_0^l v dx \sim \frac{\varepsilon}{\sqrt{u_0}} \pi$ (where l the distance between the minimum and maximum of v, for example $l = 1$ in Figure 2(a)), so that

$$u_0 \sim \left(\frac{\varepsilon \pi}{la}\right)^2. \tag{2.13}$$

In the outer region, $v \sim 0$, so that u satisfies: $Du_{xx} - a \sim 0$. Matching with the inner region, we have $u(0) = u_0$. It follows that

$$u \sim u_0 - \frac{a}{2D}\left((x-l)^2 - l^2\right). \tag{2.14}$$

In summary, the half-spike on domain $[0, l]$ has the profile

$$v(x) \sim \left(\frac{al}{\varepsilon\pi}\right)^2 \begin{cases} 1 + \cos\left(\frac{\pi}{al} x\right), & 0 \le x < al \\ 0, & \text{otherwise} \end{cases}; \quad u(x) \sim \left(\frac{\varepsilon\pi}{la}\right)^2 - \frac{a}{2D}(x-l). \tag{2.15}$$

The assumption $v \gg 1$ and $u_0 \ll 1$ then implies $a \gg \varepsilon$; at the same time for the spike to be localized we must also have $a \ll 1$. In short, the above asymptotic construction is valid provided that:

$$0 < \varepsilon \ll a \ll 1, \tag{2.16}$$

with other parameters (D and l) being $O(1)$. In fact, as we will show in Section 2.2, critical stability thresholds occur when $a = O(\varepsilon^{2/3})$ which is consistent with (2.16). Figure 1 (c and d) shows the comparison between the asymptotics (2.15) and the full steady state as obtained by numerical simulations.

2.2. *Stability*

Half-spike. We start by studying the stability of a single boundary half-spike on domain of size $(0, l)$. Linearize around the steady state constructed above as follows:

$$v(x,t) = v(x) + \phi(x) e^{\lambda t}, \quad u(x,t) = u(x) + \psi(x) e^{\lambda t}$$

to obtain

$$\lambda\phi = \varepsilon^2 \phi_{xx} + \phi u + \psi v - \left(\frac{1}{1+v}\right)^2 \phi; \quad 0 = D\psi_{xx} - \phi u - \psi v. \tag{2.17}$$

as $\hat{y} \to -\infty$. For large $\hat{y}$ we assume $\hat{V} \to 0$ so that $\hat{V}_{\hat{y}\hat{y}} \sim \hat{V}$, yielding $\hat{V}(y) \sim C \exp(-\hat{y})$ for some constant C. This provides a well-defined connection for the transition (corner) layer, between the inner and outer solution. We do not pursue it further here because it contributes only higher order terms overall; it does not affect either the profile or stability (to leading order).

https://doi.org/10.1017/jnw.2026.10038 Published online by Cambridge University Press

In the inner region $y = x\frac{\sqrt{u_0}}{\varepsilon}$ we approximate $\psi \sim \psi_0 = \psi(0)$, $\phi(x) = \Phi(y)$ and $v \sim \frac{1}{u_0}V(y)$. We obtain,

$$\lambda_0\Phi \sim \Phi_{yy} + \Phi + \frac{V}{u_0^2}\psi_0, \quad \lambda_0 = \lambda/u_0, V(y) = 1 + \cos y, \quad y \in [0, \pi]\,. \tag{2.18}$$

To match the outer solution where $\phi \sim 0$, we impose a point constraint

$$\Phi(\pi) = 0.$$

We integrate the equation for ψ in (2.17) to obtain ψ_0 :

$$\psi_0 \sim -\frac{u_0^2}{\pi}\int_0^\pi \Phi(y)dy.$$

This yields the following *non-local eigenvalue problem* (NLEP):

$$\begin{cases} \lambda_0\Phi = \Phi_{yy} + \Phi - \kappa\,(1+\cos y)\int_0^\pi \Phi(y)dy, \\ \Phi'(0) = 0; \quad \Phi(\pi) = 0. \end{cases} \tag{2.19}$$

where $\kappa = \frac{1}{\pi}$. The problem (2.19) is studied rigorously in Section 3. In particular, Theorem 3.1 states that the eigenvalues are stable ($\mathrm{Re}\,(\lambda_0) \le 0$ for all λ_0) as long as $\kappa \ge \kappa_0 = \frac{2}{3\pi}$, and are unstable otherwise. Here, $\kappa = \frac{1}{\pi} > \frac{2}{3\pi}$. This proves that a single boundary spike is stable.

Two boundary spikes. Next, consider the configuration consisting of two boundaries on the domain $[0, 2l]$ as illustrated in Figure 2. This configuration admits two distinct eigenvalues, depending on the parity of the eigenfunction with respect to the centre of the domain, as illustrated in Figure 2. If the eigenfunction is even with respect to the centre, this is equivalent to the stability of a single half-spike on the domain $[0, l]$ and was shown to be stable. On the other hand, an odd eigenfunction is equivalent to solving the eigenvalue problem (2.17) with boundary conditions $\psi(\pm l) = 0 = \phi(\pm l)$. The inner problem for Φ is the same (2.19); but now $\phi_0 = \phi(0)$ satisfies

$$\psi_{xx} = 0; \quad \psi(l) = 0, \quad D\psi'(0^+) = \frac{\varepsilon}{\sqrt{u_0}}\left(u_0\int_0^\pi \Phi dy + \psi_0\frac{\pi}{u_0}\right)$$

We obtain $\psi(x) = \psi'(0)\,(x - l)\,, \quad \psi_0 \sim -l\psi'(0^+)$ so that

$$\psi_0 = -l^2\frac{a}{D\pi}\left(u_0\int_0^\pi \Phi dy + \psi_0\frac{\pi}{u_0}\right). \tag{2.20}$$

We then obtain the problem (2.19) but with

$$\kappa = \frac{1}{\pi}\frac{D^{-1}l^4a^3\,(\varepsilon\pi)^{-2}}{1 + D^{-1}l^4a^3\,(\varepsilon\pi)^{-2}}. \tag{2.21}$$

The stability boundary corresponds to setting $\kappa = \kappa_0 = \frac{2}{3\pi}$, corresponding to the threshold $D^{-1}l^4a^3\,(\varepsilon\pi)^{-2} = 2$, or $a = a_c$ where

$$a_c = \varepsilon^{2/3}D^{1/3}l^{-4/3}2^{1/3}\pi^{2/3}. \tag{2.22}$$

By Theorem 3.1, when $a > a_c$, the two boundary spikes are stable, and they are unstable when $a < a_c$.

https://doi.org/10.1017/jnw.2026.10038 Published online by Cambridge University Press

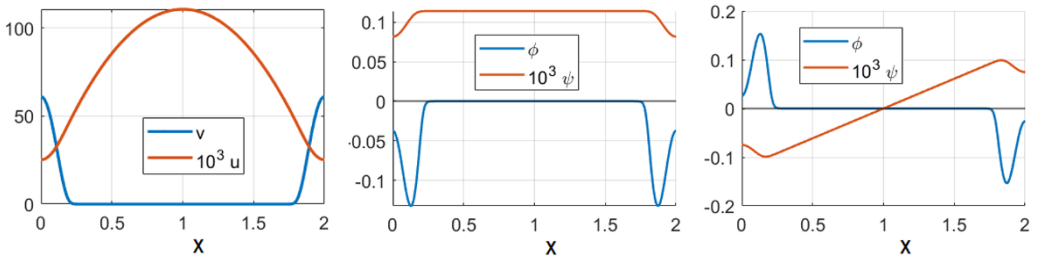


Figure 2. *Left: Steady state consisting of two boundary spikes. Here,* $A = 0.2$, $\varepsilon = 0.01$, $D = 1$ *and domain size is* $[0, 2]$ *(correspondingly,* $l = 1$ *is the distance between the maximum and the minimum of a spike). Middle: even eigenfunction corresponding to BC* $\phi'(l) = 0$. *Right: odd eigenfunction corresponding to BC* $\phi(l) = 0$.

Multiple interior spikes. Next, we consider N spikes on the domain of size $L = 2lN$, with periodic boundary conditions. We fix the domain $x \in [-l, (2l-1)N]$ and put the spikes at locations $x = 2lk, k = 0 \ldots N-1$. There are small and large eigenvalues to compute [15, 45].

Small eigenvalues. We start with the small eigenvalues that correspond to translational modes. Instead of the full computation of the small eigenvalues, we will short-circuit the process and only compute asymmetric spike solutions following [22, 43]. The point where the asymmetric branch bifurcates off the symmetric configuration corresponds to the simultaneous zero-crossing of $N-1$ small eigenvalues [43].

From (2.15), we have:

$$u(l) \sim u_0 + \frac{a}{2D} l^2 \sim \left(\frac{\varepsilon\pi}{a}\right)^2 \frac{1}{l^2} + \frac{a}{2D} l^2$$

The function $l \to u(l)$ attains a minimum when

$$-2\left(\frac{\varepsilon\pi}{a}\right)^2 \frac{1}{l^3} + \frac{a}{D} l = 0.$$

Solving for a, we obtain the same formula as in (2.22). This is precisely the bifurcation point of zero-crossing of small eigenvalues, at which all N small eigenvalues cross zero simultaneously [43]. This shows that the stability threshold of two interior boundary spikes on domain of size $4l$ (due to small eigenvalues) is exact same as the stability threshold of two boundary spikes on the domain of size $2l$ (due to large eigenvalues). It is notable that the classical systems such as Gierer–Meinhardt or Schnakenberg models exhibit exactly the same equality of stability thresholds. Finally, we let $l = L/(2N)$ to obtain the threshold for N spikes on domain of size L. The small eigenvalues are all stable when $a > a_c$ and are all unstable when $a < a_c$.

Large eigenvalues. To compute large eigenvalues on the periodic domain, we consider the eigenvalue problem (2.17) but subject to the 'Floquet' boundary conditions:

$$\psi(l) = e^{i\theta}\psi(-l), \quad \psi'(l) = e^{i\theta}\psi'(-l)$$

and similar for ϕ. Extend ψ on the entire domain by setting $\psi(x) = e^{i\theta}\psi(x-2l)$. Then $\psi((2l-1)N) = e^{i\theta N}\psi(-l)$. By choosing

$$\theta = 2\pi m/N, \quad m = 0 \ldots N-1,$$

https://doi.org/10.1017/jnw.2026.10038 Published online by Cambridge University Press

we obtain periodic boundary conditions on the entire domain. It remains to solve for ψ_0. This is equivalent to solving

$$\begin{cases} \psi'' = c\boldsymbol{\delta}(x) \\ \psi(l) = e^{i\theta}\psi(-l), \quad \psi'(l) = e^{i\theta}\psi'(-l) \end{cases} \tag{2.23}$$

where $\boldsymbol{\delta}(x)$ is the delta function and

$$c = 2l\frac{a}{D\pi}\left(u_0\int_0^{\pi}\Phi dy + \psi_0\frac{\pi}{u_0}\right)$$

This is equivalent to solving $\psi'' = 0$ with jump condition $\psi'(0^+) - \psi'(0^-) = c$ and continuity condition $\psi(0^+) = \psi(0^-)$. After some algebra we find that

$$\psi(0) = \frac{cl}{\cos(\theta) - 1} = -\frac{cl}{2\sin^2(\theta/2)}. \tag{2.24}$$

We then obtain (2.19) with the premultiplier κ being equal to

$$\kappa = \frac{1}{\pi}\frac{\left(D\sin^2(\theta/2)\right)^{-1} l^4 a^3 (\varepsilon\pi)^{-2}}{1 + \left(D\sin^2(\theta/2)\right)^{-1} l^4 a^3 (\varepsilon\pi)^{-2}}. \tag{2.25}$$

Setting $\kappa = 2/3/\pi$ yields the critical threshold

$$a_m = a_c \sin^{2/3}\left(\frac{2\pi m}{N}\right). \tag{2.26}$$

where a_c is given in (2.5). Note that $a_m \le a_c$ for all m, so that all of the thresholds a_m are below the threshold a_c that triggers the small eigenvalues. In this sense, the situation is the same as for the Schnakenberg and other related models: the instability is first triggered by small eigenvalues, as a is decreased.

2.3. Self-replication

Next, we study the phenomenon of spike self-replication. This phenomenon is observed in numerous other reaction-diffusion models. See for example [6, 8, 18, 20, 21, 30–32, 34, 36] and references therein. The path to self-replication corresponds to a disappearance of the steady state via a fold-point bifurcation [31]. At the bifurcation point, there is typically the so-called 'core problem' [8, 20, 30, 34] near the spike centre, which must be solved numerically, then matched to the outer region. Near the fold point, the solution branch connects a single spike to a double-spike structure. As we now show, a similar structure (but with a somewhat different core problem) occurs for model (2.9).

We start by looking at the inner region of the spike located at $x = 0$. Rescale:

$$x = ay, \quad u = \varepsilon^2 a^{-2} U, \quad v = \varepsilon^{-2} a^2 V, \quad D_0 = D\varepsilon^2 a^{-4}.$$

Assuming v large, the leading-order inner problem becomes

$$V_{yy} - 1 + UV = 0, \quad D_0 U_{yy} - UV \sim 0. \tag{2.27}$$

https://doi.org/10.1017/jnw.2026.10038 Published online by Cambridge University Press

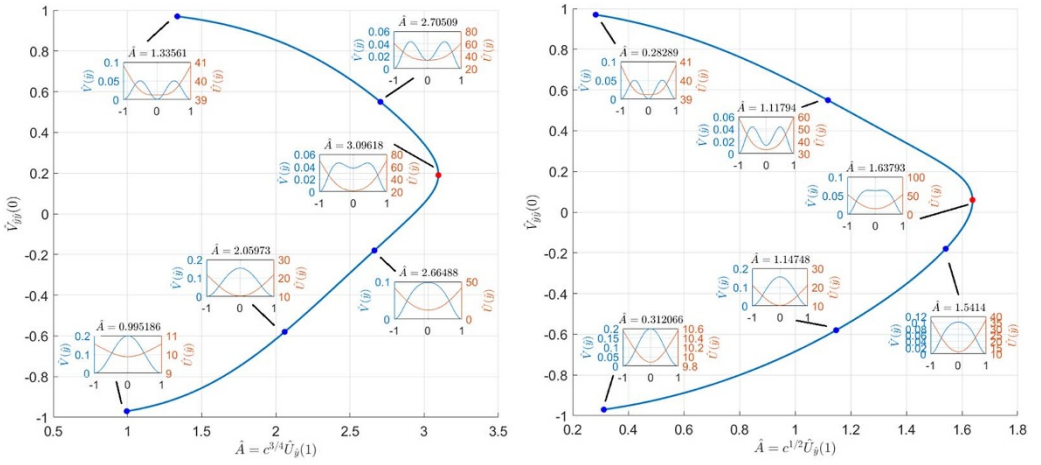


Figure 3. *(a) Bifurcation diagram for the core problem (2.29). There is a fold point at $\hat{A} = \hat{A}_s = 3.0918$ which is responsible for self-replication. (b) Bifurcation diagram for the core problem (4.10). The fold point is at $\hat{A} = \hat{A}_s = 1.6379$.*

The inner problem for $V(y)$ is defined for $y \in [0, R]$ where R is the inner domain length that is necessary to solve for. In order to match the outer region, we impose boundary conditions

$$V'(0) = 0 = U'(0); \quad V(R) = 0 = V'(R);$$

The matching condition is obtained by integrating the equation for U in (2.27). We have: $U'(R) = \frac{1}{D_0}\int_0^R UVdy \sim \frac{1}{aD_0}\int_0^l uvdx$. On the other hand, integrating (2.30) we have $\int_0^l uvdx = al$. We thus obtain the matching condition

$$U_y(\infty) = l/D_0. \tag{2.28}$$

Together, equations (2.27, 2.28) form a closed system that determines V, U as well as R as a function of system parameters. Next, we further scale to remove R as follows:

$$y = R\hat{y}, \quad V = R^2\hat{V}, \quad U = R^{-2}\hat{U}$$

to arrive at the problem

$$\hat{V}_{yy} - 1 + \hat{U}\hat{V} = 0, \quad c\hat{U}_{\hat{y}\hat{y}} - \hat{U}\hat{V} = 0 \tag{2.29a}$$

where $c = D\varepsilon^2 a^{-4} R^{-4}$. The boundary conditions become

$$\hat{V}'(0) = 0 = \hat{U}'(0); \quad \hat{V}(1) = 0 = \hat{V}'(1). \tag{2.29b}$$

Condition (2.28) then becomes $\hat{U}_{\hat{y}}(1) = R^3 l/D_0$. Eliminating R, we get $\hat{U}_{\hat{y}}(1) = c^{-3/4} l D^{-1/4} \varepsilon^{-1/2} a$. Let $\hat{A} = c^{3/4}\hat{U}_{\hat{y}}(1)$. The matching then becomes

$$\hat{A} := c^{3/4}\hat{U}_{\hat{y}}(1) = lD^{-1/4}\varepsilon^{-1/2}a. \tag{2.29c}$$

Numerically, we find that the system (2.29) has a fold point at $\hat{A} = \hat{A}_s \approx 3.0962$. This is illustrated in Figure 3(a), where we plot $\hat{A}$ versus $\hat{V}_{yy}(0)$. The two branches connect a single spike to a double spike

https://doi.org/10.1017/jnw.2026.10038 Published online by Cambridge University Press

solution and are responsible for the self-replication observed in the numerics. When $\hat{A}$ is increased past $\hat{A}_s$, the steady state is lost, and self-replication occurs.

We summarize the results as follows.

Proposition 2.1. *Consider a symmetric N−spike pattern for the model (2.29) on the domain of size L, and let $l = L/(2N)$. Let*

$$a_s = \varepsilon^{1/2} D^{1/4} l^{-1} \hat{A}_s \text{ where } \hat{A}_s \approx 3.0962, \tag{2.30}$$

$$a_c = \varepsilon^{2/3} D^{1/3} l^{-4/3} 2^{1/3} \pi^{2/3}. \tag{2.31}$$

When $N \geq 2$, the N−spike pattern is stable when $a \in (a_c, a_s)$. Self-replication is triggered when a increases past a_s and competition (spike death) is triggered when a decreases past a_c. When $N = 1$, a single spike is stable when $\varepsilon \ll a < a_s$.

3. Nonlocal eigenvalue problem

Here, we rigorously study the stability of the key NLEP problem (2.19):

$$\begin{cases} \lambda_0 \Phi = \Phi_{yy} + \Phi - \kappa w \int_0^\pi \Phi(y) dy, \quad w(y) = 1 + \cos(y) \\ \Phi'(0) = 0; \quad \Phi(\pi) = 0. \end{cases} \tag{3.1}$$

We have the following characterization of stability for the operator (3.1).

Theorem 3.1. *Let $\kappa_0 = \frac{2}{3\pi}$. The following thresholds phenomenon holds:*

- *If $\kappa > \kappa_0$, then all eigenvalues of (3.1) are strictly stable, i.e. $\mathrm{Re}\,(\lambda_0) < 0$ for all λ_0.*
- *If $\kappa = \kappa_0$, then there exists one zero eigenvalue and the rest of eigenvalues are strictly stable, $\mathrm{Re}\,(\lambda_0) < 0$.*
- *Suppose that $\kappa < \kappa_0$. Then there exists a real positive eigenvalue $\lambda_0 > 0$.*

Note that the operator in (3.1) is not self-adjoint and in general the eigenvalues can be complex, which complicates the analysis. We will follow the ideas of the method introduced in [44]. The idea is to 'self-adjointize' the operator.

In what follows, we write $\int = \int_0^\pi dy$. Let w_0, κ_0 be the solution to (3.1) corresponding to the zero eigenvalue, namely

$$w_0'' + w_0 - \kappa_0 w \int w_0 = 0.$$

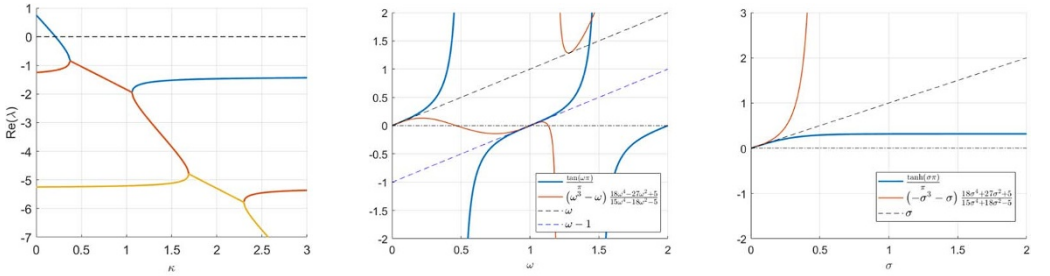
Explicitly, we have

$$w_0(y) = \cos y + 1 + \frac{1}{2} y \sin y; \quad \kappa_0 = \frac{1}{\int w_0} = \frac{2}{3\pi}.$$

Now define the operator

$$L_1 \Phi := \Phi'' + \Phi - \kappa_0 w \int \Phi - \kappa_0 \int w \Phi + \kappa_1 \int \Phi \tag{3.2}$$

https://doi.org/10.1017/jnw.2026.10038 Published online by Cambridge University Press



(a) (b) (c)

Figure 4. *(a) Spectrum of the eigenvalue problem (3.1) computed numerically. Note the zero-crossing at* $\kappa = \kappa_0 = \frac{2}{3\pi}$ *of the principal eigenvalue. The problem is stable for* $\kappa_0 > \frac{2}{3\pi}$*, despite having complex eigenvalues. (b) Plot of (3.3). (c) Plot of (3.4).*

where κ_1 is chosen such that $L_1 w_0 = 0$:

$$0 = -\kappa_0 \int w w_0 + \kappa_1 \int w_0,$$
$$\kappa_1 = \kappa_0 \frac{\int w w_0}{\int w_0} = \frac{5}{6\pi}.$$

Lemma 3.2. *The operator* L_1 *is self-adjoint and non-positive definite.*

Proof. An explicit computation shows that the eigenvalues of L_1 satisfy

$$\frac{\tan(\omega\pi)}{\pi} = \left(\omega^3 - \omega\right) \frac{18\omega^4 - 27\omega^2 + 5}{15\omega^4 - 18\omega^2 - 5}, \quad \lambda = 1 - \omega^2 \tag{3.3}$$

Since L_1 is self-adjoint, λ is purely real. So there are two cases to consider: either ω is purely real or it is purely imaginary.

Case 1, ω is purely real. The graph of lhs and rhs of (3.3) is shown in Figure 4(b). As can be seen from the graph, there are no roots when $\omega \in (0,1)$. This is easy to prove rigorously as follows. Let $f(\omega) = rhs(3.3)$. Then for $\omega \in (0,1)$, $f(\omega)$ is below the line $y = \omega$ and above the line $y = \omega - 1$. Indeed, a simple computation shows $f(\omega) = \omega$ is equivalent $\left(3\omega^2 - 5\right)^2 = 0$ which has no roots in $(0,1)$. Similarly, setting $f(w) = \omega - 1$ one obtains $18\omega^4 + 54\omega^3 + 48\omega^2 + 15\omega + 5 = 0$, which again has no roots for $\omega > 0$ as all the coefficients are positive.

Case 2, $\omega = i\sigma$ with σ purely real. Then equation (3.3) becomes

$$\frac{\tanh(\sigma\pi)}{\pi} = \left(-\sigma^3 - \sigma\right) \frac{18\sigma^4 + 27\sigma^2 + 5}{15\sigma^4 + 18\sigma^2 - 5} \tag{3.4}$$

The graph of (3.4) is shown in Figure 4(c) and shows that there are no non-zero solutions to (3.4). This is easily shown using the same arguments as in Case 1 (and is left to the reader). This completes the proof of the lemma. □

https://doi.org/10.1017/jnw.2026.10038 Published online by Cambridge University Press

We are now ready to prove Theorem **3.1.**

Proof of Theorem 3.1

To show the instability when $\kappa < \kappa_0$, we solve (3.1) explicitly to find that λ_0 satisfies

$$\frac{\tan(\omega\pi)}{\pi\left(\omega-\omega^3\right)} = 1 - \frac{\omega^2}{\kappa\pi}, \quad \lambda_0 = 1-\omega^2. \tag{3.5}$$

Simple calclulus shows that (3.5) has a root $\omega \in (0,1)$ when $\kappa < \kappa_0$ (in fact $\omega = 1$ corresponds to $\kappa = \kappa_0$). This shows the existence of a positive (and real) eigenvalue of (3.1) when $\kappa < \kappa_0$.

Next, we show stability when $\kappa \geq \kappa_0$. Write (3.1) as

$$\lambda_0\Phi = L_1\Phi + (\kappa_0-\kappa)\, w\int \Phi + \kappa_0 \int w\Phi - \kappa_1 \int \Phi$$

Decompose $\lambda_0 = \lambda_R + i\lambda_I$, $\Phi = \Phi_R + i\Phi_I$; so that

$$\lambda_R\Phi_R - \lambda_I\Phi_I = L_1\Phi_R + (\kappa_0-\kappa)\, w\int \Phi_R + \kappa_0 \int w\Phi_R - \kappa_1 \int \Phi_R \tag{3.6}$$

$$\lambda_R\Phi_I + \lambda_I\Phi_R = L_1\Phi_I + (\kappa_0-\kappa)\, w\int \Phi_I + \kappa_0 \int w\Phi_I - \kappa_1 \int \Phi_I \tag{3.7}$$

The combination $\int \Phi_R \int (3.6) + \int \Phi_I \int (3.7)$ yields:

$$\begin{aligned}\lambda_R\left\{\left(\int \Phi_R\right)^2 + \left(\int \Phi_I\right)^2\right\} = \left\{\int \Phi_R L_1\Phi_R + \Phi_I L_1\Phi_I\right\} + (\kappa_0-\kappa-\kappa_1)\,\pi\left\{\left(\int \Phi_R\right)^2 + \left(\int \Phi_I\right)^2\right\} \\ + \kappa_0\pi\left\{\int \Phi_R w\int \Phi_R + \int \Phi_I w\int \Phi_I\right\}\end{aligned} \tag{3.8}$$

Note that

$$\int w\left(\Phi'' + \Phi\right) = \int \Phi\left(w'' + w\right) = \int \Phi.$$

Multiplying (3.6, 3.7) by w, integrating and eliminating λ_I therefore yields

$$\lambda_R\left\{\left(\int w\Phi_R\right)^2 + \left(\int w\Phi_I\right)^2\right\} = \left(1-\kappa\int w^2\right)\left\{\int \Phi_R w\int \Phi_R + \int \Phi_I w\int \Phi_I\right\}. \tag{3.9}$$

Eliminate $\int w\Phi_R \int \Phi_R + \int w\Phi_I \int \Phi_I$ between (3.8) and (3.9) to obtain

$$\lambda_R(A) - \kappa_0\pi\lambda_R B\frac{1}{\left(1-\kappa\int w^2\right)} = \left\{\int \Phi_R L_1\Phi_R + \Phi_I L_1\Phi_I\right\} + (\kappa_0-\kappa-\kappa_1)\,\pi A$$

where

$$A = \left\{\left(\int \Phi_R\right)^2 + \left(\int \Phi_I\right)^2\right\}, \quad B = \left\{\left(\int \Phi_R w\right)^2 + \left(\int \Phi_I w\right)^2\right\}.$$

https://doi.org/10.1017/jnw.2026.10038 Published online by Cambridge University Press

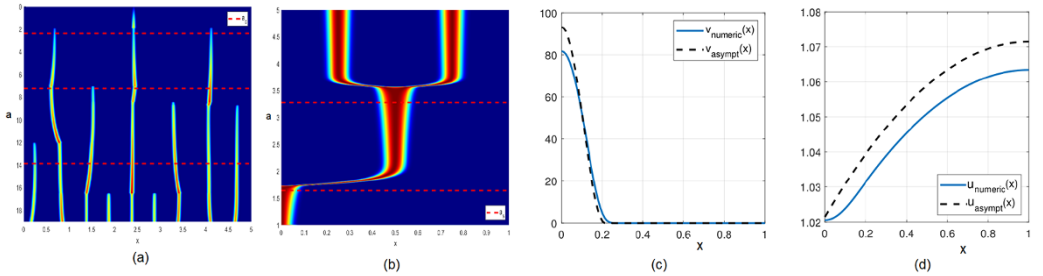


Figure 5. *(a) Competition instability for model (4.1). Here, $D = 100, \varepsilon = 0.0025$, $L = 5$, and a is gradually decreased according to $a = 20(1 - 10^{-5}t)$. Dashed lines indicate the asymptotic prediction a_c (4.12) for $N = 9, 6$, and 3 spikes. Colouration is normalized at each time slice, with deep red corresponding to a maximum and deep blue corresponding to zero. (b) Spike self-replication. Here, $D = 1, L = 1, \varepsilon = 0.005$. Dashed lines indicate the asymptotic prediction a_s (4.11) for $N = 1/2$ and $N = 1$ spikes. (c) and (d) Half-spike steady state of (4.1). Panel (c) shows v and panel (d) shows u. Here, $D = 100$, $a = 10$, $\varepsilon = 0.01$, $l = 1$. Dashed lines indicate asymptotics (4.2, 4.3, 4.4).*

Using the fact that $\int w^2 = 1/\kappa_0$, we get

$$\lambda_R \left(A + \frac{4}{9\pi} \frac{1}{\kappa - \kappa_0} B \right) = \left\{ \int \Phi_R L_1 \Phi_R + \Phi_I L_1 \Phi_I \right\} + (\kappa_0 - \kappa - \kappa_1)\, \pi A$$

Now $A, B > 0$ whereas the right hand side is always negative when $\kappa > \kappa_0$. This shows $\lambda_R < 0$ whenever $\kappa > \kappa_0$. ■

4. Schnakenberg model with saturation

We now perform a similar analysis for the Schnakenberg model with saturation (1.2). After some scaling, we write it in the form

$$v_t = \varepsilon^2 v_{xx} - v + \frac{v}{1+v} uv, \quad 0 = Du_{xx} + a - uv. \tag{4.1}$$

We simplified the model assuming k_2 is negligible, and further assumed that the plant population changes on a slower scale than the precipitation in the soil (hence zero instead of u_t). We first construct the steady state, then analyse its stability.

As before, we will assume that u and v decouple in the inner region, and start by constructing a single boundary spike on domain $[0, l]$. In the inner region, u is assumed to be nearly constant, and turns out to be very close to 1, whereas v is large. Setting $u(x) \sim 1 + \delta$, where δ is a small constant to be determined, the equilibrium for v becomes

$$0 = \varepsilon^2 v_{xx} + \delta v + (1 + \delta) \left(-1 + \frac{1}{1+v} \right).$$

Assuming v large we estimate $(1 + \delta) \left(-1 + \frac{1}{1+v} \right) \sim -1$. We then find, as in Section 2,

$$v(x) \sim \frac{1}{\delta} \begin{cases} \left(1 + \cos\left(x \frac{\sqrt{\delta}}{\varepsilon} \right) \right), & |x| < \pi \frac{\varepsilon}{\sqrt{\delta}} \\ 0, & |x| > \pi \frac{\varepsilon}{\sqrt{\delta}} \end{cases} \tag{4.2}$$

https://doi.org/10.1017/jnw.2026.10038 Published online by Cambridge University Press

To find δ, we integrate $\int_0^l (a - uv)dx = 0$ which yields

$$\delta = \varepsilon^{2/3} \left(\frac{\pi}{al}\right)^{2/3}. \tag{4.3}$$

Stability computation is also very similar to Section 2. We compute that

$$u(x) \sim 1 + \delta - \frac{a}{2D}(x - l)^2 + \frac{a}{2D}l^2, \quad \delta^{2/3} \ll x < l \tag{4.4}$$

so that

$$u(l) = 1 + \delta + \frac{a}{2D}l^2 \sim 1 + \varepsilon^{2/3} \left(\frac{\pi}{a}\right)^{2/3} l^{-2/3} + \frac{a}{2D}l^2.$$

The function $l \to u(l)$ attains a minimum when

$$\frac{2}{3}\varepsilon^{2/3} \left(\frac{\pi}{a}\right)^{2/3} l^{-5/3} = 2\frac{a}{2D}l. \tag{4.5}$$

Solving (4.5) for a, we obtain the stability threshold $a = a_c$ given by (4.12). The pattern is unstable if $a < a_c$ and is is stable for $a > a_c$. For large eigenvalues, we linearize around the steady state to obtain the eigenvalue problem

$$\lambda\phi = \varepsilon^2\phi_{xx} + \phi\left((u - 1) - \frac{u}{(1 + v)^2}\right) + \left(-1 + v + \frac{1}{1 + v}\right)\psi, \quad 0 = D\psi_{xx} - \phi u - \psi v. \tag{4.6}$$

The corresponding NLEP problem is identical to (2.19) but with the following κ :

$$\kappa = \frac{1}{\pi}\varepsilon^{-2/3} \left(\frac{\pi}{al}\right)^{-2/3} \text{ for a single boundary spike on } (0, l)$$

$$\kappa = \frac{l^2 a}{D}\frac{1}{\pi}\varepsilon^{-2/3} \left(\frac{\pi}{al}\right)^{-2/3} \text{ for double boundary spike on } (0, 2l)$$

$$\kappa = \frac{l^2 a}{D\sin^2(\theta/2)}\frac{1}{\pi}\varepsilon^{-2/3} \left(\frac{\pi}{al}\right)^{-2/3}, \ m = 1 \ldots N - 1 \text{ for } N\text{spikes on domain of size } 2lN.$$

As before, the stability boundary corresponds to $\kappa = \kappa_0 = \frac{2}{3\pi}$. So no surprise here: we have the usual situation that the small eigenvalues are destabilized before large ones, and therefore (4.12) gives the competition instability threshold.

Finally, we derive the self-replication thresholds. We rescale,

$$u(x) = 1 + \varepsilon^{2/3}U(y), \quad v(x) = \frac{1}{\varepsilon^{2/3}}V(y), \quad x = \varepsilon^{2/3}y.$$

We then obtain, at leading order, a coupled *core problem*

$$V_{yy} + VU - 1 = 0, \qquad DU_{yy} - V = 0. \tag{4.7}$$

Similar to (2.1), the inner problem for $V(y)$ is defined for $y \in [0, R]$ where R is the inner domain length that is necessary to solve for through additional constraints

$$V'(0) = 0 = U'(0) \ \text{ and } \ V(R) = V'(R) = 0. \tag{4.8}$$

https://doi.org/10.1017/jnw.2026.10038 Published online by Cambridge University Press

The matching condition is obtained by integrating the equation for U in (4.7). We have: $U'(R) = \frac{1}{D}\int_0^R V(y)dy \sim \frac{1}{D}\int_0^l v(x)dx$. On the other hand, integrating (4.1) we have $\int_0^L uvdx \sim \int_0^L vdx = al$. We thus obtain the matching condition

$$U'(R) = \frac{al}{D}. \tag{4.9}$$

Together, equations (4.7, 4.8, 4.9) form a closed system that determines V, U as well as R as a function of system parameters. Next, we further scale to remove R as follows:

$$y = R\hat{y}, \quad V = R^2\hat{V}, \quad U = \frac{1}{R^2}\hat{U}, \quad c = \frac{D}{R^6}.$$

The resulting system is

$$\hat{V}_{\hat{y}\hat{y}} + \hat{V}\hat{U} - 1 = 0, \qquad c\hat{U}_{\hat{y}\hat{y}} - \hat{V} = 0; \tag{4.10a}$$

$$\hat{V}'(0) = 0 = \hat{U}'(0); \quad \hat{V}(1) = \hat{V}'(1) = 0 \tag{4.10b}$$

whereas equation (4.9) becomes

$$\hat{A} = \hat{U}'(1)\sqrt{c}, \quad \text{where } \hat{A} = \frac{al}{\sqrt{D}}. \tag{4.10c}$$

For each c, the system (4.10) is solved numerically. Numerically, we find a fold point at $\hat{A} = \hat{A}_s = 1.638$. This is illustrated in Figure 3, where we plot $\hat{A}$ versus $\hat{V}_{yy}(0)$. The two branches connect a single spike to a double spike solution and are responsible for the self-replication observed in the numerics.

We summarize the results as follows.

Theorem 4.1. *Consider a symmetric $N-$spike pattern for the model (4.1) on the domain of size L, and let $l = L/(2N)$. Let*

$$a_s = D^{1/2}l^{-1}\hat{A}_{\max} \text{ where } \hat{A}_s \approx 1.638, \tag{4.11}$$

$$a_c = D^{3/5}\varepsilon^{2/5}l^{-8/5}(2/3)^{3/5}\pi^{2/5}. \tag{4.12}$$

When $N \geq 2$, the $N-$spike pattern is stable when $a \in (a_c, a_s)$. Self-replication is triggered when a increases past a_s and competition (spike death) is triggered when a decreases past a_c. When $N = 1$, a single spike is stable when $\varepsilon \ll a < a_s$.

5. Discussion

We studied the effect of saturation on localized pattern formation for systems (1.1), (1.2). To our knowledge, this is the first time that the asymptotics and stability of localized patterns have been studied for the mussel–algae model 1.1). In contrast to numerous previous studies where the spike have a profile of the form of sech to some power, the spike studied here has a cosine-type profile (2.15) and leads to novel NLEP problem (3.1).

https://doi.org/10.1017/jnw.2026.10038 Published online by Cambridge University Press

Our techniques apply to a wide range of reaction-diffusion systems in the presence of saturation. Another example is a variant of Macarthur–Rosenzweig type model with an Allee effect for the predator, similar to [1]:

$$N_t = d_1 N_{xx} + k_1 N - k_2 N^2 - k_3 NP, \quad P_t = d_2 P_{xx} - k_4 P + \frac{k_5 P}{k_6 P + k_7} NP \tag{5.1}$$

Here, N and P are populations of prey and predator, respectively. The predator-prey interactions are modulated by the predator Allee effect $\frac{k_5 P}{k_6 P + k_7}$, which allows for spatial pattern formation. It is very similar to the model (1.2) except that the constant production is replaced by a logistic growth term. This makes the outer problem non-linear. It would be interesting to study how this changes the dynamics and stability of localized patterns.

There are numerous open questions for future study. These include: spot dynamics, oscillatory instabilities and construction of stripes and spots in higher dimensions. In two dimensions, we expect the spot profile to be described by a Bessel J function. It would be interesting to extend the stability analysis of Section 2.2 to this context. On the other hand, stable stripe solutions have also been observed in numerical simulations of the mussel–algae model in 2D when the drift terms are added to algae [27]. It was shown in [19] that drift can indeed lead to stripe stabilization for the classical Schnakenberg model. It would be interesting to attempt a similar analysis for the mussel–algae model.

Funding statement. S.X. is supported by the NSFC China (Grant No. 12401198).

T.K. is supported by the NSERC Discovery Grant, Canada.

J. Wei is partially supported by the National Key R&D Program of China (No. 2022YFA1005602), and the Hong Kong General Research Fund 'New frontiers in singular limits of nonlinear partial differential equations'.

References

[1] **Akhtar SK, Peet AB and Peacock-Lopez E** (2012) Complex dynamics in a modified Macarthur–Rosenzweig model with predator paring. *Journal of Biological Systems* **20**(01), 87–108.

[2] **Barrio R, Varea C, Aragón J and Maini P** (1999) A two-dimensional numerical study of spatial pattern formation in interacting turing systems. *Bulletin of Mathematical Biology* **61**(3), 483–505.

[3] **Benson DL, Maini PK and Sherratt JA** (1998) Unravelling the turing bifurcation using spatially varying diffusion coefficients. *Journal of Mathematical Biology* **37**(5), 381–417.

[4] **Cangelosi RA, Wollkind DJ, Kealy-Dichone BJ and Chaiya I** (2015) Nonlinear stability analyses of turing patterns for a mussel-algae model. *Journal of Mathematical Biology* **70**, 1249–1294.

[5] **Chaturapruek S, Breslau J, Yazdi D, Kolokolnikov T and McCalla SG** (2013) Crime modeling with lévy flights. *SIAM Journal on Applied Mathematics* **73**(4), 1703–1720.

[6] **Chen C-C and Kolokolnikov T** (2012) Simple PDE model of spot replication in any dimension. *SIAM Journal on Mathematical Analysis* **44**(5), 3564–3593.

[7] **Chen Y, Kolokolnikov T, Tzou J and Gai C** (2015) Patterned vegetation, tipping points, and the rate of climate change. *European Journal of Applied Mathematics* **26**(06), 945–958.

[8] **Doelman A, Kaper TJ and Peletier LA** (2006) Homoclinic bifurcations at the onset of pulse self-replication. *Journal of Differential Equations* **231**(1), 359–423.

[9] **Doelman A, Kaper TJ and Zegeling PA** (1997) Pattern formation in the one-dimensional Gray–Scott model. *Nonlinearity* **10**(2), 523.

[10] **Gai C and Kolokolnikov T** (2023) Resource-mediated competition between two plant species with different rates of water intake. *SIAM Journal on Applied Mathematics* **83**(2), 576–602.

[11] **Ge Z** (2023) The hidden order of turing patterns in arid and semi-arid vegetation ecosystems. *Proceedings of the National Academy of Sciences* **120**(42), e2306514120.

[12] **Grall E and Tschopp P** (2020) A sense of place, many times over-pattern formation and evolution of repetitive morphological structures. *Developmental Dynamics* **249**(3), 313–327.

[13] **Guttal V and Jayaprakash C** (2007) Self-organization and productivity in semi-arid ecosystems: Implications of seasonality in rainfall. *Journal of Theoretical Biology* **248**(3), 490–500.

[14] **Ibanez J and Velarde M** (1978) Multiple steady states in a simple reaction–diffusion model with Michaelis–Menten (first-order Hinshelwood–Langmuir) saturation law: The limit of large separation in the two diffusion constants. *Journal of Mathematical Physics* **19**(1), 151–156.

https://doi.org/10.1017/jnw.2026.10038 Published online by Cambridge University Press

[15] **Iron D, Ward MJ and Wei J** (2001) The stability of spike solutions to the one-dimensional Gierer–Meinhardt model. *Physica D: Nonlinear Phenomena* **150**(1), 25–62.
[16] **Iron D, Wei J and Winter M** (2004) Stability analysis of turing patterns generated by the Schnakenberg model. *Journal of Mathematical Biology* **49**, 358–390.
[17] **Klausmeier CA** (1999) Regular and irregular patterns in semiarid vegetation. *Science* **284**(5421), 1826–1828.
[18] **Kolokolnikov T and Tlidi M** (2007) Spot deformation and replication in the two-dimensional Belousov-Zhabotinski reaction in a water-in-oil microemulsion. *Physical Review Letters* **98**(18), 188303.
[19] **Kolokolnikov T, Ward M, Tzou J and Wei J** (2018) Stabilizing a homoclinic stripe, Philosophical Transactions of the Royal Society A: Mathematical. *Physical and Engineering Sciences* **376**(2135), 20180110.
[20] **Kolokolnikov T, Ward MJ and Wei J** (2005) The existence and stability of spike equilibria in the one-dimensional Gray–Scott model: The pulse-splitting regime. *Physica D: Nonlinear Phenomena* **202**(3-4), 258–293.
[21] **Kolokolnikov T, Ward MJ and Wei J** (2009) Spot self-replication and dynamics for the Schnakenburg model in a two-dimensional domain. *Journal of Nonlinear Science* **19**(1), 1–56.
[22] **Kolokolnikov T, Ward MJ and Wei J** (2014) The stability of steady-state hot-spot patterns for a reaction-diffusion model of urban crime. *Discrete & Continuous Dynamical Systems-Series B* **19**(5), 1373.
[23] **Kolokolnikov T and Wei J** (2018) Pattern formation in a reaction-diffusion system with space-dependent feed rate. *SIAM Review* **60**(3), 626–645.
[24] **Kondo S and Asai R *et al*** (1995) A reaction-diffusion wave on the skin of the marine angelfish pomacanthus. *Nature* **376**(6543), 765–768.
[25] **van de Koppel J, Rietkerk M, Dankers N and Herman PM** (2005) Scale-dependent feedback and regular spatial patterns in young mussel beds. *The American Naturalist* **165**(3), E66–E77.
[26] **Landge AN, Jordan BM, Diego X and Müller P** (2020) Pattern formation mechanisms of self-organizing reaction-diffusion systems. *Developmental Biology* **460**(1), 2–11.
[27] **Liu Q-X, Weerman EJ, Herman PM, Olff H and van de Koppel J** (2012) Alternative mechanisms alter the emergent properties of self-organization in mussel beds. *Proceedings of the Royal Society B: Biological Sciences* **279**, 2744–2753.
[28] **Maini PK, Woolley TE, Baker RE, Gaffney EA and Lee SS** (2012) Turing's model for biological pattern formation and the robustness problem, Interface focus. rsfs20110113.
[29] **Muratov C** (2002) Theory of domain patterns in systems with long-range interactions of coulomb type. *Physical Review E* **66**(6), 066108.
[30] **Muratov C and Osipov VV** (2000) Static spikeautosolitons in the Gray–Scott model. *Journal of Physics A: Mathematical and General* **33**(48), 8893.
[31] **Nishiura Y and Ueyama D** (1999) A skeleton structure of self-replicating dynamics. *Physica D: Nonlinear Phenomena* **130**(1), 73–104.
[32] **Nishiura Y and Ueyama D** (2001) Spatio-temporal chaos for the Gray–Scott model. *Physica D: Nonlinear Phenomena* **150**(3), 137–162.
[33] **Nogare DD and Chitnis AB** (2017) Self-organizing spots get under your skin. *PLoS Biology* **15**(12), e2004412.
[34] **Pearson JE** (1993) Complex patterns in a simple system. *Science* **261**(5118), 189–192.
[35] **Peng R, Shi J and Wang M** (2008) On stationary patterns of a reaction–diffusion model with autocatalysis and saturation law. *Nonlinearity* **21**(7), 1471.
[36] **Reynolds WN, Ponce-Dawson S and Pearson JE** (1997) Self-replicating spots in reaction-diffusion systems. *Physical Review E* **56**(1), 185.
[37] **Rietkerk M, Boerlijst MC, Van Langevelde F, HilleRisLambers R, v. de Koppel J, Kumar L, Prins HH and de Roos AM** (2002) Self-organization of vegetation in arid ecosystems. *The American Naturalist* **160**(4), 524–530.
[38] **Saadi FA, Champneys A, Gai C and Kolokolnikov T** (2022) Spikes and localised patterns for a novel Schnakenberg model in the semi-strong interaction regime. *European Journal of Applied Mathematics* **33**(1), 133–152.
[39] **Sherratt JA** (2005) An analysis of vegetation stripe formation in semi-arid landscapes. *Journal of Mathematical Biology* **51**(2), 183–197.
[40] **Sherratt JA and Lord GJ** (2007) Nonlinear dynamics and pattern bifurcations in a model for vegetation stripes in semi-arid environments. *Theoretical Population Biology* **71**(1), 1–11.
[41] **Short MB, Dorsogna MR, Pasour VB, Tita GE, Brantingham PJ, Bertozzi AL and Chayes LB** (2008) A statistical model of criminal behavior. *Mathematical Models and Methods in Applied Sciences* **18**(supp01), 1249–1267.
[42] **Wang R-H, Liu Q-X, Sun G-Q, Jin Z and van de Koppel J** (2009) Nonlinear dynamic and pattern bifurcations in a model for spatial patterns in young mussel beds. *Journal of the Royal Society Interface* **6**(37), 705–718.
[43] **Ward MJ and Wei J** (2002) The existence and stability of asymmetric spike patterns for the Schnakenberg model. *Studies in Applied Mathematics* **109**(3), 229–264.

https://doi.org/10.1017/jnw.2026.10038 Published online by Cambridge University Press

[44] **Wei J** (1999) On single interior spike solutions of the Gierer–Meinhardt system: uniqueness and spectrum estimates. *European Journal of Applied Mathematics* **10**(4), 353–378.
[45] **Wei J and Winter M** (2013) *Mathematical Aspects of Pattern Formation in Biological Systems* Vol. **189**. Springer Science & Business Media.
[46] **Zipkin JR, Short MB and Bertozzi AL** (2014) Cops on the dots in a mathematical model of urban crime and police response. *Discrete Contin. Dyn. Syst. Ser. B* **19**(5), 1479–1506.

Cite this article: Kolokolnikov T, Xie S and Wei J (2026) Localized pattern formation for mussel–algae model and other reaction-diffusion systems with saturation. *Journal of Nonlinear Waves*, 1–18. https://doi.org/10.1017/jnw.2026.10038

https://doi.org/10.1017/jnw.2026.10038 Published online by Cambridge University Press